Journal of Magnetic Resonance 309 (2019) 106594

Contents lists available at ScienceDirect

Journal of Magnetic Resonance

journal homepage: www.elsevier.com/locate/jmr

Polarization of low-γ nuclei by transferring spin order of parahydrogen at high magnetic fields

Vitaly P. Kozinenko, Alexey S. Kiryutin, Alexandra V. Yurkovskaya, Konstantin L. Ivanov *

International Tomography Center, Siberian Branch of the Russian Academy of Sciences, Novosibirsk 630090, Russia
Novosibirsk State University, Novosibirsk 630090, Russia

ARTICLE INFO

Article history:
Received 18 May 2019
Revised 6 September 2019
Accepted 7 September 2019
Available online 19 September 2019

ABSTRACT

In this work, we optimize the performance of a previously proposed method for transferring parahydrogen induced polarization to "insensitive" spin-1/2 NMR (Nuclear Magnetic Resonance) nuclei, which have low gyromagnetic ratio and low natural abundance. By optimizing the reaction conditions and pressure of the parahydrogen gas and using adiabatically switched radiofrequency fields we achieve high polarization transfer efficiency and report carbon spin polarization of dimethyl acetylene dicarboxylate reaching 35%, which corresponds to ^{13}C NMR signal enhancements of about 43,000 at 9.4 Tesla. Such polarization levels allow one to work with mM concentrations at natural carbon abundance and to detect ^{13}C NMR signal in single scan. In combination with a pseudo phase cycle, the polarization transfer method used here also enables efficient suppression of unwanted background signals.

1. Introduction

Nuclear Magnetic Resonance (NMR) spectroscopy is a powerful and versatile analytical method widely used in chemistry, biomedicine, and other fields. However, low polarization of nuclear spin systems at thermal equilibrium conditions significantly limits the sensitivity of the method. This issue is of great importance for NMR spectroscopy of nuclei with low gyromagnetic ratios and low natural abundance (e.g., ^{13}C or ^{15}N): it is common that hundreds or even thousands of signal acquisitions are required to achieve a sufficient signal-to-noise ratio. One of the most efficient approaches to enhance weak NMR signals is given by generating strong non-equilibrium polarization of nuclear spin system, termed spin hyperpolarization. Presently, there are a number of hyperpolarization methods known for amplifying NMR signals by several orders of a magnitude: dynamic nuclear polarization [1–3], optical pumping [4–6], chemically induced dynamic nuclear polarization [7–9], optical nuclear polarization [10–12], quantum rotor induced polarization [13,14] and parahydrogen induced polarization [15,16].

In Parahydrogen Induced Polarization (PHIP) signal amplification originates from symmetry breaking in parahydrogen (pH_2, the H_2 molecule in its nuclear singlet state) in the course of a catalytic hydrogenation reaction [15,16]. The achievable NMR signal enhancement factors, ε, for protons in PHIP experiments reach up to 4 orders of magnitude. Hence, PHIP is an efficient hyperpolarization technique; moreover, it is relatively cheap and simple in use. An important application of PHIP is transfer of polarization from primarily polarized protons to "insensitive" magnetic nuclei, such as ^{13}C or ^{15}N, which have a lower gyromagnetic ratio and natural abundance. At the same time, these nuclei typically have much longer T_1 and T_2 relaxation times as compared to protons, being promising MRI contrast agents, once their NMR signals are sufficiently strong.

There are two main methods for transferring PHIP to heteronuclei: "spontaneous" polarization transfer at ultralow magnetic fields [17–22], usually combined with magnetic field cycling, and polarization transfer in a high magnetic field of an NMR spectrometer driven by radiofrequency (RF) pulses [23]. The former method is known for high transfer efficiency but it requires dedicated equipment for generating low or even ultralow (down to several 100 nT) magnetic fields and also for performing fast and reproducible sample transport to the high NMR detection field. The latter method is easier to combine with conventional high-field NMR experiments but optimization of the polarization transfer efficiency is an important issue. Previous experiments report enhancements reaching several thousands to 20,000. For instance, INEPT-type (INEPT = Insensitive Nuclei Enhanced by Polarization Transfer [24]) pulse sequences enable ^{13}C signal enhancement of the order of $\varepsilon = 5000$ [25]. The use of a special pulse sequence for low-field PHIP [26] provides 20% of ^{13}C-polarization of succinic acid in experiments performed at the 1.76 mT field [27]. Recently,

* Corresponding author at: International Tomography Center, Siberian Branch of the Russian Academy of Sciences, Novosibirsk 630090, Russia.
E-mail address: ivanov@tomo.nsc.ru (K.L. Ivanov).

https://doi.org/10.1016/j.jmr.2019.106594
1090-7807/

carbon NMR enhancements reaching $\varepsilon = 20,000$ have been reported [28], achieved by exploiting optimized INEPT-based sequences, revealing the great potential of NMR methods using coherence transfer. Eills et al. [29] have demonstrated PHIP-derived ^{13}C NMR enhancement of the order of 9,000 using 50% enriched pH_2: the achieved spin order transfer efficiency would correspond to $\varepsilon \approx 23,000$ with 90% pH_2.

In this work, we use a double frequency RF-excitation method to transfer PHIP to ^{13}C nuclei at high fields [30,31]. This method has been suggested earlier [30,31] and it allows one transferring the singlet order of protons to carbon spins by adiabatic passage through Level Anti-Crossings (LACs) in the rotating reference frame. This technique can be implemented on any modern NMR spectrometer having a double-frequency H-X probe and does not require any additional devices, e.g., for performing magnetic field cycling. The efficiency of the technique depends on the parameters of the two RF-fields, i.e., on their amplitudes and frequencies. Moreover, as the method exploits a ramped RF-field in the carbon channel, optimization of the RF-pulse envelope allows one to reduce the duration of the sequence, thus preventing unwanted polarization losses from spin relaxation. Additionally, we optimize the reaction conditions by increasing the pH_2 pressure. This optimization strategy is designated to increase further the carbon signal enhancement, which was about 6,000 in the original publication [30].

As a result, we can demonstrate that the optimization allows one to achieve the ^{13}C polarization reaching 35.2%, which is equivalent to the enhancement factor of $\varepsilon = 43,200$ for ^{13}C nuclei. Furthermore, implementation of a pseudo phase cycle with variable excitation frequency on the carbon channel enables efficient suppression of background signals.

2. Materials and methods

2.1. Sample preparation

In NMR experiments, we used a 5 mm NMR tube filled with a solution of a substrate (dimethyl acetylenedicarboxylate) and a hydrogenation catalyst (1,4-bis(diphenylphosphino)butane(1,5-cyclooctadiene)Rh(I) tetrafluoroborate) in 0.6 ml of acetone d_6. To run repetitive experiments for optimization of experimental conditions, e.g., those aimed at measuring the RF-frequency dependence of carbon polarization, we used a solution with a low concentration of the catalyst (0.2 mM) and high concentration of the substrate (0.4 M). In the experiments aimed at reaching the highest enhancement with optimized RF-parameters, we used a solution containing 5 mM of the catalyst and 6 mM of the substrate in order to hydrogenate all substrate molecules in a single experiment by adding pH_2 into the solution.

2.2. PHIP experiments

To generate PHIP we used a gas supply system for NMR operating at high pressure, as described in Ref. [32]. Bubbling at high pressure allows one to increase the concentration of pH_2 in the solution and thus to reach higher enhancement levels. In the present case, the gas pressure was 4 bars, and the temperature of the sample was kept equal to 298 K. To obtain the H_2 gas enriched in its *para*-component, we used a Bruker parahydrogen generator, which produces the H_2 gas with 92% of the *para*-isomer. In the course of homogeneous catalytic hydrogenation with pH_2, the dimethyl acetylenedicarboxylate molecule turns into maleic acid dimethyl ester with two hyperpolarized protons prepared in the singlet state, see Fig. 1. In this study, we focus on transferring this hyperpolarization to the ^{13}C nuclei denoted C_A and C_B, see Fig. 1. These nuclei are present at natural abundance of the ^{13}C isotope, which is equal to 1%; hence, in most molecules there are no ^{13}C nuclei or only a single ^{13}C-spin, C_A or C_B.

2.3. Polarization transfer scheme

To transfer polarization from protons to ^{13}C nuclei we implemented a double frequency RF-excitation scheme [30] presented in Fig. 2. The experimental protocol is as follows. First, we bubble pH_2 through the solution during a time period of $\tau_b = 10$ s. Then, a waiting time $\tau_w = 0.5$ s is introduced to reduce inhomogeneity of the sample caused by bubbling. Subsequently, we turn on RF-excitation on both proton and carbon channels. The amplitude of the RF-field of protons stays constant being equal to ν_1^H, while the amplitude of the ^{13}C RF-field, ν_1^C, is adiabatically decreased from the maximal value to zero during the time τ_{off}. The ^1H RF-field is applied on resonance with the two protons originating from pH_2, $\nu_0^H = \nu_{RF}^H$, while the frequency of the ^{13}C RF-field, ν_{RF}^C, is shifted (by less than 500 Hz) from the resonance frequency of the carbon nucleus of interest. Finally, to detect the ^{13}C NMR spectrum we apply a hard 90-degree RF-pulse on the ^{13}C channel and perform the Fourier transform on the resulting FID (Free Induction Decay) signal.

2.4. Theory

To explain how the pulse sequence shown in Fig. 2 works, we use the concept of LACs (Level Anti Crossings) and introduce the spin Hamiltonian in the doubly rotating reference frame [30]. We describe the polarized product molecule as a 3-spin system with two spins of the chemically equivalent protons, $\mathbf{I}_1$ and $\mathbf{I}_2$, and a single ^{13}C spin, denoted as $\mathbf{S}$. The Hamiltonian of the spin system in the lab frame in the absence of RF-excitation is as follows:

$$\hat{\mathcal{H}}_0 = -\nu_0^H\left\{\hat{I}_{1z} + \hat{I}_{2z}\right\} - \nu_0^C\hat{S}_z + J_{12}\left(\hat{\mathbf{I}}_1 \cdot \hat{\mathbf{I}}_2\right) + J_{1S}\left(\hat{\mathbf{I}}_1 \cdot \hat{\mathbf{S}}\right) + J_{2S}\left(\hat{\mathbf{I}}_2 \cdot \hat{\mathbf{S}}\right) \quad (1)$$

Here we use the following J-coupling values: $J_{12} = 11.5$ Hz, $J_{1S} = 168$ Hz, $J_{2S} = 2$ Hz for the C_A nucleus and $J_{12} = 11.5$ Hz, $J_{1S} = 13.7$ Hz, $J_{2S} = 0$ for the C_B nucleus; ν_0^H and ν_0^C are the NMR frequencies of the protons and ^{13}C nucleus.

After turning on the RF-fields (directed along the x-axis in the rotating reference frame), we rewrite the Hamiltonian, omitting the rapidly oscillating terms as done previously [30]. Here we go to the rotating frame for each kind of nucleus. As the proton RF-field is directly on resonance with the two protons, $\nu_H^{RF} = \nu_H^0$, the Hamiltonian is as follows:

$$\hat{\mathcal{H}}_{DRF}(t) = -\{\nu_0^C - \nu_{RF}^C\}\hat{S}_z + J_{12}\left(\hat{\mathbf{I}}_1 \cdot \hat{\mathbf{I}}_2\right) + J_{1S}\hat{I}_{1z}\hat{S}_z + J_{2S}\hat{I}_{2z}\hat{S}_z - \nu_1^H\left(\hat{I}_{1x} + \hat{I}_{2x}\right) - \nu_1^C(t)\hat{S}_x \quad (2)$$

Hence, the Zeeman interactions of the nuclei are modified; in the terms describing heteronuclear couplings we keep only the products of the z-projections of the spin operators (the proton-proton coupling term remains the same as in Eq. (1)).

In the present case, the function $\nu_1^C(t)$ describes the time-dependent ^{13}C RF-field. By adiabatically decreasing the amplitude of the carbon RF-field, we transfer the population of the singlet state of the protons into the magnetization of the carbon nucleus. In the case of adiabatic RF-field variation, we correlate the spin states before and after the switch and the singlet state population is transferred selectively to a target spin state, which gives rise to hyperpolarization of the carbon spin [30]. The choice of an appropriate target spin state is performed by setting the carbon

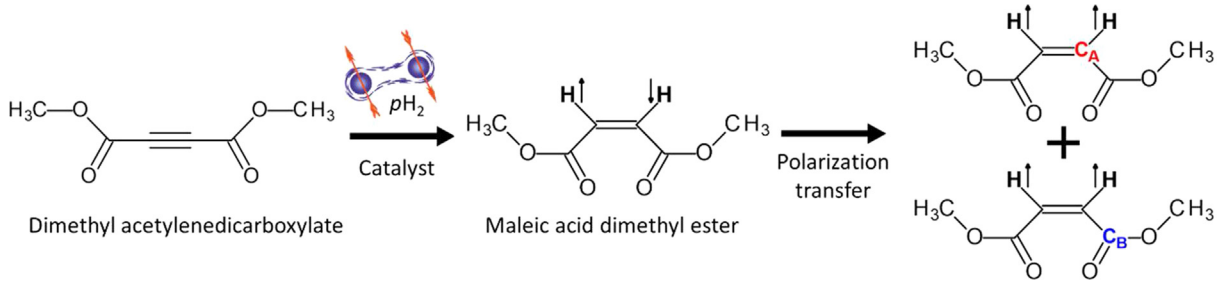

Fig. 1. Catalytic hydrogenation of dimethyl acetylenedicarboxylate producing maleic acid dimethyl ester. The two highlighted protons in the product originate from the pH_2 molecule. The polarization is transferred from pH_2 protons to one of ^{13}C nuclei denoted as C_A and C_B.

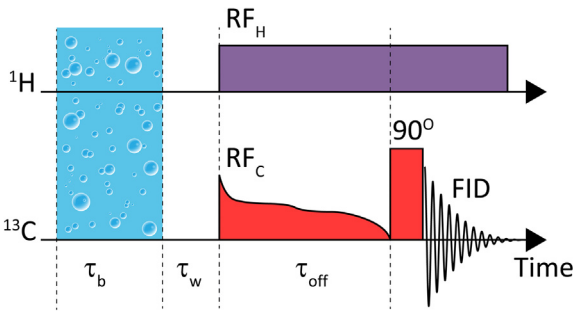

Fig. 2. Pulse sequence for polarization transfer from protons to ^{13}C nuclei. The ^{1}H RF-field, RF_H, stays constant during the experiment, while the ^{13}C RF-field, RF_C, is adiabatically decreased from the maximal value to zero. In this work, we optimized the time profile of the $\nu_1^C(t)$ RF-field.

RF-frequency, i.e., of the off-set value, $\delta\nu_C = \nu_0^C - \nu_{RF}^C$. To fulfill the adiabaticity condition passage through LAC regions (see Figs. 3a and 4a) must be slow enough, so that the populations follow the energy levels during the variation of the Hamiltonian. However, simple increase of the switching time is not always a suitable strategy, since relaxation kicks-in during the switch and significantly reduces the spin order. A better way to implement adiabatic RF-field variation is to optimize the switching profile in order to (a) minimize the time and (b) keep a high degree of adiabaticity. Qualitatively, this can be achieved by passing through the LAC regions slowly and introducing fast passage in-between LACs. Quantitatively, such an adiabatic process can be introduced by performing a switch keeping constant the generalized adiabaticity parameter [33,34]. To do so, we define the adiabaticity parameter for a pair of adiabatic states $|i\rangle$ and $|j\rangle$, which change in time upon variation of the Hamiltonian:

$$\xi_{ij} = \frac{1}{2\pi\nu_{ij}}\left\langle i\left|\frac{d}{dt}\right|j\right\rangle, \tag{3}$$

where $\nu_{ij} = E_i - E_j$, with E_i and E_j denoting the i-th and j-th eigenvalues of the Hamiltonian. Adiabaticity is fulfilled, when $\xi_{ij} \ll 1$, i.e., when time variation of the eigen-states is much slower than the internal evolution of the system. The key idea of constant adiabaticity is that the Hamiltonian should be varied slowly within LAC regions, where the splitting between the energy levels is small (i.e., ν_{ij} is small) and state mixing occurs (i.e., the derivative $\frac{d}{dt}|j\rangle$ is large), and fast outside LACs. Hence, to achieve constant adiabaticity we decrease the RF-field variation rate at LAC regions and increase it outside LAC regions. Such a method allows one to reduce the total switching time and thus to implement "fast" adiabatic switching [33,34].

To calculate the optimal profile for $\nu_1^C(t)$ we rewrite the adiabaticity parameter as follows:

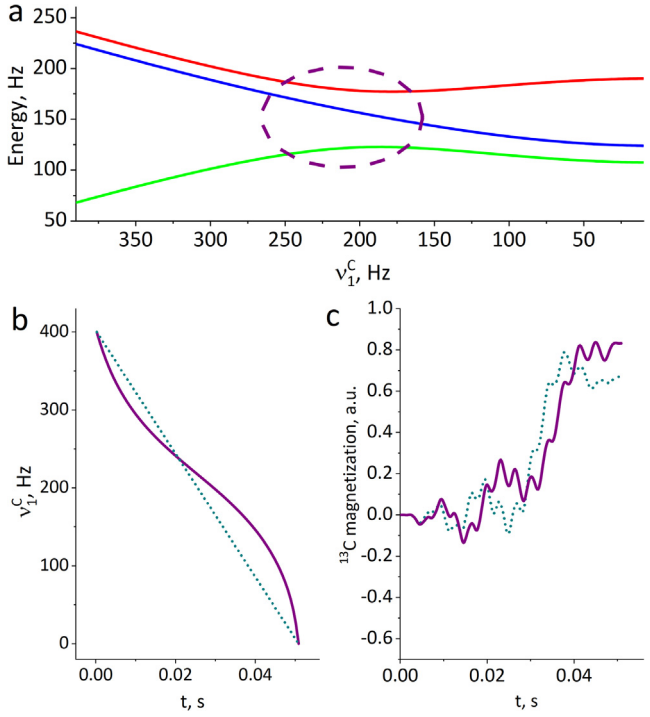

Fig. 3. Energy levels of the spin system as a function of the ^{13}C RF field amplitude, ν_1^C, in the case of transfer to the C_A nucleus (subplot a). Linear profile (dots) and profile with "constant adiabaticity" (solid line) of the RF-field variation (subplot b). Subplot c: polarization of the C_A nucleus for linear profile (dots) and profile with "constant adiabaticity" (solid line) as a function of time. For both profiles, the simulation parameters were as follows: $\tau_{off} = 0.05$ s, $\nu_1^C(t=0) = 400$ Hz, $\nu_{RF}^C = 134$ ppm, $\nu_1^H = 300$ Hz, $\nu_{RF}^H = 6.36$ ppm. Dashed circle in (a) indicates the LAC region.

$$\xi_{ij}(t) = \frac{1}{(2\pi\nu_{ij})^2}\left\langle i\left|\frac{d\widehat{\mathcal{H}}_{DRF}(t)}{dt}\right|j\right\rangle = \text{const} \tag{4}$$

and take the average of the $\xi_{ij}(t)$ values for all pairs of states of the spin system:

$$\langle\xi\rangle(t) = \sqrt{\sum_{ij}\xi_{ij}^2(t)}. \tag{5}$$

Since

$$\frac{d\widehat{\mathcal{H}}_{DRF}(t)}{dt} = \frac{d\nu_C^1(t)}{dt}\cdot\widehat{S}_x$$

we can rewrite Eq. (4) as an ordinary differential equation for $\nu_1^C(t)_x$ and solve it numerically, by assuming $\langle\xi\rangle(t) = \text{const}$. This procedure has been described in detail in previous works and RF-field profiles with "constant adiabaticity" appear to be very efficient for generating singlet order in pairs of coupled spins [30].

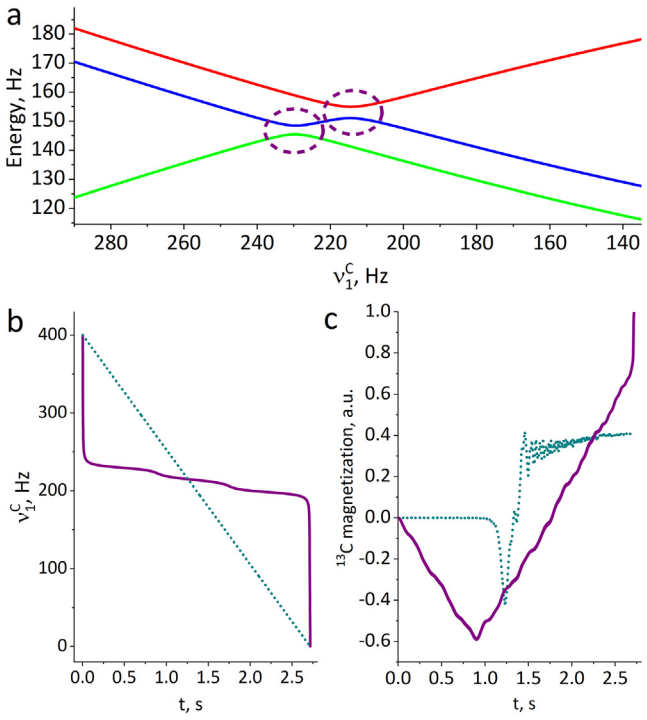

Fig. 4. Energy levels of the spin system as a function of the ^{13}C RF field amplitude ν_1^C in the case of transfer to the C_B nucleus (subplot a). Linear profile (dots) and profile with "constant adiabaticity" (solid line) of the RF-field variation (subplot b). Subplot c: polarization of the C_B nucleus for linear profile (dots) and profile with "constant adiabaticity" (solid line) as a function of time. For both profiles, the simulation parameters were as follows: $\tau_{off} = 2.6$ s, $\nu_1^C(t=0) = 400$ Hz, $\nu_{RF}^C = 134$ ppm, $\nu_1^H = 300$ Hz, $\nu_{RF}^H = 6.36$ ppm. Dashed lines in (a) indicate the LAC regions.

Figs. 3 and 4 (see subplots a) present the appearance of the relevant LACs for three-spin systems of two protons and a carbon spin, being C_A or C_B nuclei. We also show linear and optimal profiles of $\nu_1^C(t)$ (see subplots b in both figures), and numerically simulated time dependence of the polarization of the carbon nucleus (see subplots c in both figures) for linear and "constant adiabaticity" profiles.

In the case of the C_A nucleus, the energy levels form a "triple" LAC with a large energy splitting defined by the proton-carbon coupling constant, $J_{1S} = 168$ Hz. Since the LAC region is broad, there is no significant difference between the linear profile and optimized profile; the transfer efficiency is also comparable for both profiles. In the case of the C_B nucleus, there are two LAC regions separated from each other. For each LAC, the minimal splitting between the levels is relatively small due to smaller proton-carbon coupling constant, $J_{1S} = 13.7$ Hz. Therefore, the optimal profile, which takes the structure of the LACs into account, has a better performance compared to the linear profile. Thus, the profile with "constant adiabaticity" enables shortening the total transfer time without sacrificing the transfer efficiency. This method can thus be exploited to decrease the switching time and to minimize polarization losses due to relaxation.

Finally in this subsection, we would like to discuss one more issue, dealing with the spin order of the two primarily polarized protons. At first glance, this issue is trivial, since we work with pH$_2$, i.e., with a pair of protons in the singlet state. Nonetheless, after pH$_2$ binds to a PHIP catalyst or to a substrate, singlet-triplet conversion may become efficient once the singlet state of H$_2$ is not an eigenstate of the spin system (the protons become magnetically or even chemically non-equivalent). In our previous works [35–37] we argue that this is indeed the case in some situations. In the present case the singlet is not an eigenstate of the hydrogenation product molecule, in particular, for the molecule containing the C_A carbon: in the absence of RF-excitation the eigenstates are to a good approximation the Zeeman basis states due to the relatively large difference of the J-couplings to the ^{13}C spin.

To prevent from the unwanted singlet-triplet mixing we have taken the following measures. The waiting time in our experiments was taken relatively short, commonly, $\tau_w = 0.5$ s. We also take the ^{1}H RF-field and the initial ^{13}C-field such that the spin system is away from the LACs shown in Figs. 3a and 4a (namely, the difference in ν_1^H and ν_1^C is always taken sufficiently large). Under such conditions the singlet state of the protons is nearly an eigenstate of the spin Hamiltonian. We also tried to turn on the proton RF-field also during bubbling of the solution with pH$_2$; however, in this case the signal enhancement was reduced by almost on order of magnitude.

As mentioned above, magnetic non-equivalence can give rise to singlet-triplet mixing, reducing the singlet order and selectively populating the triplet $|T_0\rangle$ state [35–37]. In this situation, the singlet order changes to the anti-phase order. To check whether this is indeed the case we introduced a 90-degree ^{1}H RF-pulse prior to the proton RF-excitation: such a pulse partly reconstitutes the singlet order and thus can increase the resulting NMR enhancement [36]. However, after this modification the signal enhancement has not change, which is an indication that the singlet order is not perturbed significantly. Nonetheless, modification of the spin order of H$_2$ can be an important issue in PHIP experiments, which has to be taken into account.

3. Results

The position of the LAC region and, therefore, the efficiency of polarization transfer depend on the frequency of ^{13}C RF-excitation. In the cases where the RF-frequency is very far from the resonance of the heteronucleus or is directly on resonance the transfer efficiency is zero. In the former case the matching condition $\nu_H \approx \nu_{eff}^C = \sqrt{(\nu_1^C)^2 + (\delta\nu_C)^2}$ cannot be fulfilled, while in the latter case correlation of adiabatic states in not appropriate. Generally speaking, the frequency of the ^{13}C RF-field defines, which states are correlated in the transfer process and, thus, the sign of the resulting ^{13}C magnetization (see Fig. 5). Therefore, appropriate choice of the ν_{RF}^C frequency is a necessary prerequisite for achieving the maximal carbon NMR enhancement.

The amplitude of the proton RF-field defines the range of the frequencies of the ^{13}C RF-field suitable for performing the desired polarization transfer. Using higher ν_1^H amplitudes makes it simpler to fulfill the matching condition, $\nu_1^H \approx \nu_{eff}^C$: this condition is fulfilled for a broader range of the ν_{RF}^C off-sets, see Fig. 6. However, setting a too strong RF-field also has disadvantages. First, intense RF-fields might heat the sample and give rise to convection, so that hyperpolarized molecules migrate from the detection zone reducing the observable signal enhancement. Second, in the case of too strong RF-fields, it is harder to fulfill the adiabaticity condition during transfer (the LAC regions become narrower), which results in polarization losses. Thus, it is preferable to work with moderate RF-field amplitudes (namely, 0.5 to 1 kHz).

As discussed above, the total transfer time should be set such that passage through the LACs is performed in an adiabatic manner and relaxation losses are minimized. Fig. 7 presents the τ_{off}-dependence of the polarization transfer efficiency for the C_A (subplot a) and C_B (subplot b) nuclei, obtained with both linear and optimal profiles. For the C_A nucleus the transferred polarization reaches its maximum at the switching time of 0.25 s, and the performance of the linear and optimal profiles is similar. In the case of

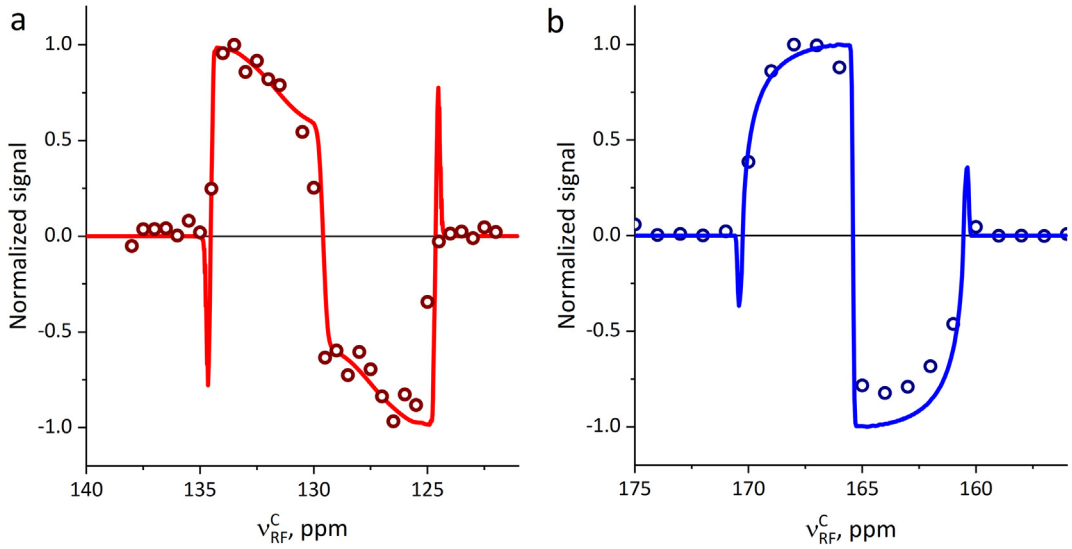

Fig. 5. Dependence of the polarization transfer efficiency on the frequency ν^C_{RF}. The amplitude ν^H_1 is equal to 500 Hz, maximum amplitude $\nu^C_1(t=0)$ is 600 Hz. Subplot a: dependence for C_A (τ_{off} = 0.5 s), subplot b: dependence for C_B (τ_{off} = 5 s). Solid lines – numerical calculation, circles – experimental data.

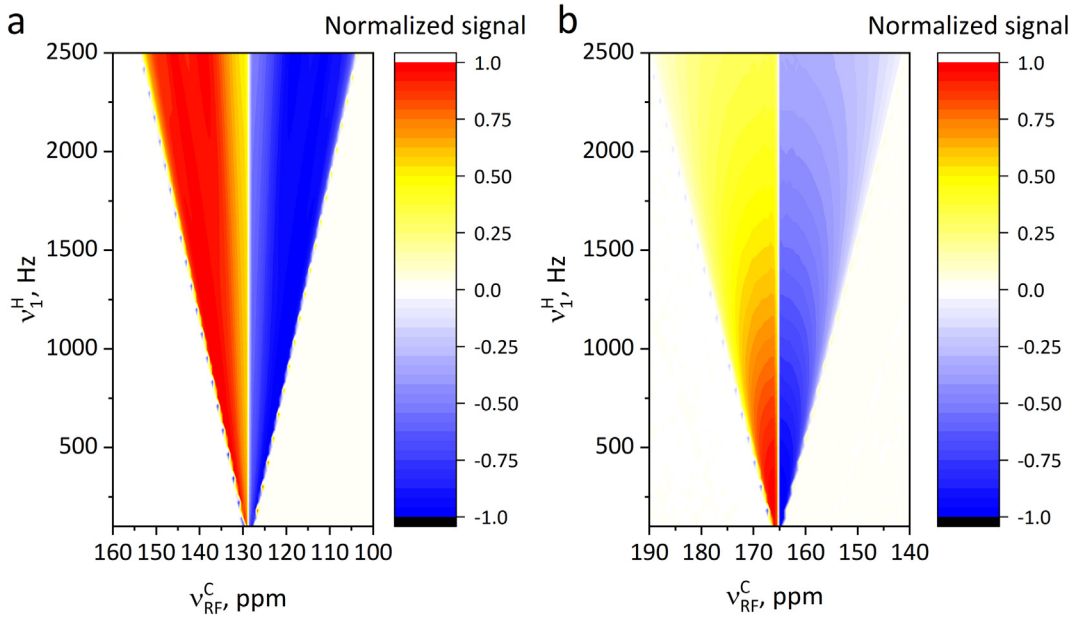

Fig. 6. Dependence of the polarization transfer efficiency on the frequency of ^{13}C RF-excitation, ν^C_{RF}, and on the amplitude ν^H_1 (numerical calculation). Subplot a: dependence for C_A ($\tau_{off} = 0.5$ s), subplot b: dependence for C_B ($\tau_{off} = 5$ s).

transfer to the C_B nucleus, the optimal τ_{off} is equal to 26 s for optimal and 38 s for linear profile. The different τ_{off} dependences for the C_A and C_B nuclei arise from the different spin-spin coupling constants between the protons and the corresponding carbon nuclei. For the C_A nucleus, the proton-carbon J_{CH} coupling constant is equal to 168 Hz, resulting in a bigger splitting at the LACs, and faster polarization transfer. For the C_B nucleus, the J_{CH} coupling constant is 13.7 Hz, so that the LAC regions are narrower, which makes the adiabaticity condition harder to fulfil during the switching. In this case, the optimal profile, which suggests slow passage through the LACs, increases the maximal efficiency of polarization transfer by 10%.

Using all possible optimization methods, we obtained a signal amplification of $\varepsilon = 43,200$ for the C_A nucleus, which corresponds to 35.2% of ^{13}C polarization, and $\varepsilon = 29,000$ for the C_B nucleus, which corresponds to 23.5% of polarization. The NMR spectra exhibiting these enhancement factors are presented in Fig. 8. One can see that the signals of the hyperpolarized molecules have significantly higher intensities than the lines of the residual ^{13}C-nuclei of the solvent.

In addition to high enhancements, we demonstrate that the method used here is suitable also for suppressing background signals. This is possible because the ^{13}C RF-field almost does not affect the thermally polarized background signals. At the same time, the sign of the carbon hyperpolarization can be controlled by the sign of the frequency offset relative to the ^{13}C Larmor frequency of the targeted nucleus, i.e., the polarization changes its sign for experiments with positive and negative $\delta\nu_C$. Hence, by subtracting the NMR spectra obtained after polarization transfer with positive and negative $\delta\nu_C$ we double the hyperpolarized signals and

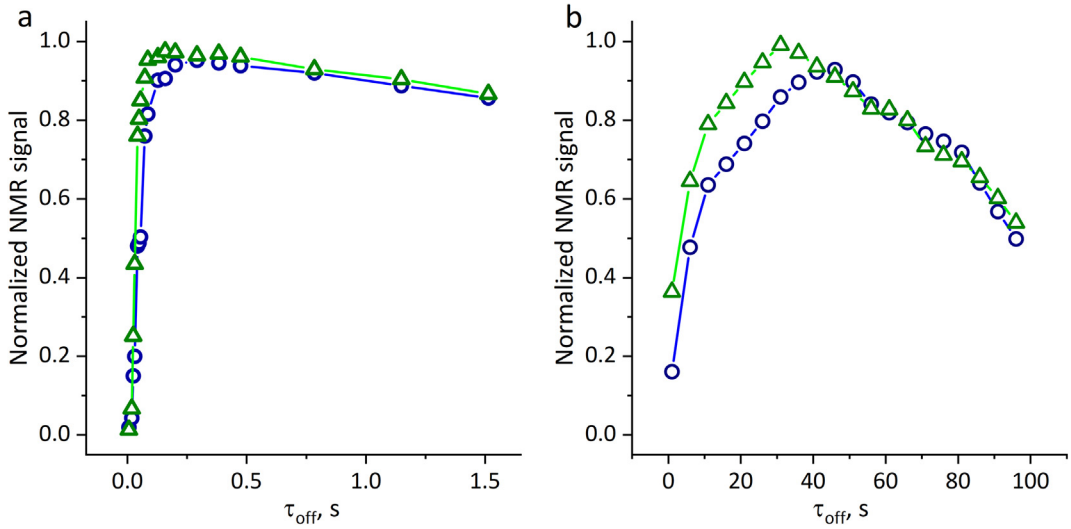

Fig. 7. Dependence of the polarization transfer efficiency on τ_{off}. Subplot a: results for C_A, subplot b: results for C_B. Circles – linear profile for ^{13}C RF excitation ramp, triangles – profile with "constant adiabaticity".

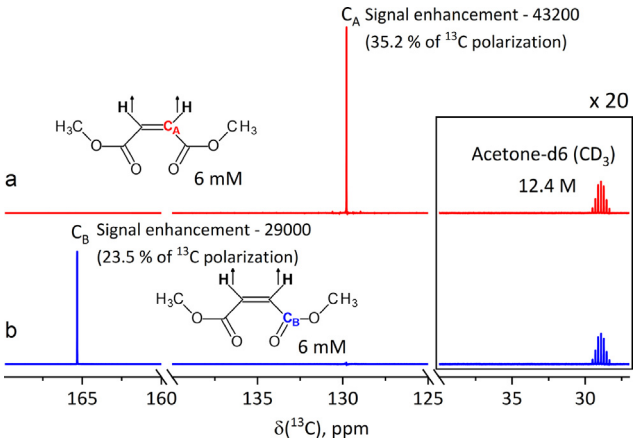

Fig. 8. Hyperpolarized NMR spectra for the C_A (subplot a) and C_B (subplot b) nuclei. The concentration of the polarized molecules is 6 mM, while the concentration of thermally polarized solvent acetone d_6 (used as a reference) is 12.5 M. Spectra are obtained after a single acquisition. In the case of transfer to C_A nucleus, the amplitude ν_1^H was equal to 500 Hz, maximum amplitude $\nu_1^C(t=0)$ was 1000 Hz. For C_B nucleus the amplitudes ν_1^H and $\nu_1^C(t=0)$ were 500 Hz and 600 Hz, respectively.

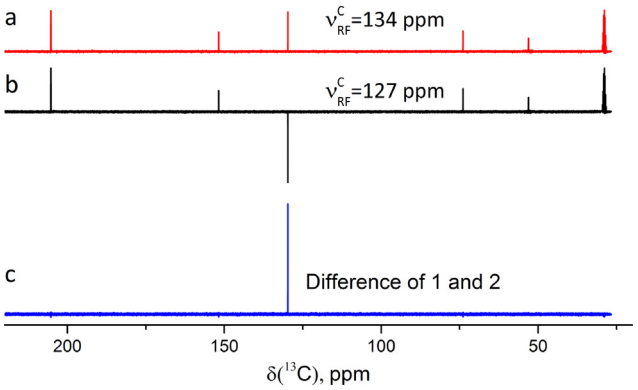

Fig. 9. ^{13}C NMR spectra of maleic acid dimethyl ester after the transfer of PHIP to C_A nucleus with ν^C_{RF} = 134 ppm (subplot a) and ν^C_{RF} = 127 ppm (subplot b). The difference of the spectra 1 and 2 demonstrates almost complete suppression of the background signals (subplot c).

subtract the thermal signals. Hence, the difference spectrum yields only the hyperpolarized signal of the nuclei of interest, while the background signals (here the solvent signals) are suppressed, see Fig. 9.

4. Conclusions

In this work we report efficient transfer of parahydrogen-derived spin order of protons to ^{13}C heteronuclei at high magnetic field. Polarization transfer at high fields occurs in the presence of RF-excitation of both protons and heteronuclei; we exploit adiabatic passage through LACs in the doubly-rotating reference frame. Following the variation of the ^{13}C RF-field, the system passes through the LACs, giving rise to efficient and selective polarization transfer. We show that using a profile with "constant adiabaticity" for RF-field envelopes increases the efficiency of PHIP transfer, especially for remote carbon the spin-spin coupling between protons and heteronulcei is not so strong (about 10 Hz). Using optimized parameters, namely, reaction conditions (catalyst concentration and pH_2 pressure) and RF-field parameters (amplitudes, frequencies, and envelopes for the ^{13}C RF-field), allowed us to obtain a 43,000-fold signal enhancement, which corresponds to 35% of ^{13}C polarization. Moreover, this method is capable of efficient suppression of background signals, which is due to the fact that the ^{13}C polarization changes its sign upon sign variation of $\delta\nu_C$. As a result, high performance of the methods exploited in this work makes them applicable for the selective detection of PHIP-polarized molecules at small concertation and natural isotope abundance. Potentially, such hyperpolarization strategies can broaden the range of analytical and diagnostic applications of PHIP.

Acknowledgements

This work has been supported by the Russian Science Foundation (grant No. 19-43-04116). We acknowledge the Russian Ministry of Science and Higher Education for providing access to NMR facilities at ITC SB RAS.

References

[1] K.H. Hausser, D. Stehlik, Dynamic nuclear polarization in liquids, in: J.S. Waugh (Ed.), Adv. Magn. Res., Academic, New York, 1968, pp. 79–139.
[2] T. Maly, G.T. Debelouchina, V.S. Bajaj, K.-N. Hu, C.-G. Joo, M.L. Mak-Jurkauskas, J.R. Sirigiri, P.C.A. van der Wel, J. Herzfeld, R.J. Temkin, R.G. Griffin, Dynamic

nuclear polarization at high magnetic fields, J. Chem. Phys. 128 (2008), 052211 (052211-052219).
[3] J.H. Ardenkjaer-Larsen, B. Fridlund, A. Gram, G. Hansson, L. Hansson, M.H. Lerche, R. Servin, M. Thaning, K. Golman, Increase in signal-to-noise ratio of > 10,000 times in liquid-state NMR, Proc. Natl. Acad. Sci. U. S. A. 100 (2003) 10158–10163.
[4] W. Happer, Optical pumping, Rev. Mod. Phys. 44 (1972) 169–249.
[5] T.G. Walker, W. Happer, Spin-exchange optical pumping of noble-gas nuclei, Rev. Mod. Phys. 69 (1997) 629.
[6] R. Tycko, S.E. Barrett, Optically Pumped NMR of Semiconductors and Two-Dimensional Electron Systems, eMagRes, John Wiley & Sons, Ltd, 2007.
[7] K.M. Salikhov, Y.N. Molin, R.Z. Sagdeev, A.L. Buchachenko, Spin Polarization and Magnetic Effects in Chemical Reactions, Elsevier, Amsterdam, 1984.
[8] M. Goez, Elucidating organic reaction mechanisms using photo-CIDNP spectroscopy, Top. Curr. Chem. 338 (2012) 1–32.
[9] O.B. Morozova, K.L. Ivanov, Time-resolved CIDNP of biologically important molecules, ChemPhysChem 20 (2018) 197–215.
[10] D. Stehlik, H.-M. Vieth, Time evolution of electron-nuclear cross-polarization in radiofrequency induced optical nuclear spin polarization (RF-ONP), in: D.M. S. Bagguley (Ed.), Pulsed Magn. Reson.: NMR, ESR, Opt., Clarendon Press, Oxford, 1992, pp. 446–477.
[11] B.M. Goodson, Applications of optical pumping and polarization techniques in NMR: I. Optical nuclear polarization in molecular crystals, Annu. Rep. NMR Spectrosc. 55 (55) (2005) 299–323.
[12] O.B. Morozova, A.V. Yurkovskaya, H.-M. Vieth, D.V. Sosnovsky, K.L. Ivanov, Light-induced spin hyperpolarisation in condensed phase, Mol. Phys. 115 (2017) 2907–2943.
[13] A.J. Horsewill, Quantum tunnelling aspects of methyl group rotation studied by NMR, Prog. Nucl. Magn. Reson. Spectrosc. 35 (1999) 359–389.
[14] B. Meier, J.N. Dumez, G. Stevanato, J.T. Hill-Cousins, S.S. Roy, P. Hakansson, S. Mamone, R.C.D. Brown, G. Pileio, M.H. Levitt, Long-lived nuclear spin states in methyl groups and quantum-rotor-induced polarization, J. Am. Chem. Soc. 135 (2013) 18746–18749.
[15] J. Natterer, J. Bargon, Parahydrogen induced polarization, Prog. Nucl. Magn. Reson. Spectrosc. 31 (1997) 293–315.
[16] R.A. Green, R.W. Adams, S.B. Duckett, R.E. Mewis, D.C. Williamson, G.G.R. Green, The theory and practice of hyperpolarization in magnetic resonance using parahydrogen, Prog. Nucl. Magn. Reson. Spectrosc. 67 (2012) 1–48.
[17] H. Jóhannesson, O. Axelsson, M. Karlsson, Transfer of para-hydrogen spin order into polarization by diabatic field cycling, C. R. Phys. 5 (2004) 315–324.
[18] M. Goldman, H. Jóhannesson, O. Axelsson, M. Karlsson, Hyperpolarization of ^{13}C through order transfer from parahydrogen: a new contrast agent for MRI, Magn. Reson. Imaging 23 (2005) 153–157.
[19] E. Cavallari, C. Carrera, S. Aime, F. Reineri, Studies to enhance the hyperpolarization level in PHIP-SAH-produced C13-pyruvate, J. Magn. Reson. 289 (2018) 12–17.
[20] M.L. Truong, T. Theis, A.M. Coffey, R.V. Shchepin, K.W. Waddell, F. Shi, B.M. Goodson, W.S. Warren, E.Y. Chekmenev, N-15 Hyperpolarization by reversible exchange using SABRE-SHEATH, J. Phys. Chem. C 119 (2015) 8786–8797.
[21] T. Theis, M.L. Truong, A.M. Coffey, R.V. Shchepin, K.W. Waddell, F. Shi, B.M. Goodson, W.S. Warren, E.Y. Chekmenev, Microtesla SABRE enables 10% nitrogen-15 nuclear spin polarization, J. Am. Chem. Soc. 137 (2015) 1404–1407.
[22] A.S. Kiryutin, A.V. Yurkovskaya, H. Zimmermann, H.-M. Vieth, K.L. Ivanov, Complete magnetic field dependence of SABRE-derived polarization Magn, Reson. Chem. 56 (2018) 651–662.
[23] J. Barkemeyer, J. Bargon, H. Sengstschmid, R. Freeman, Heteronuclear polarization transfer using selective pulses during hydrogenation with parahydrogen, J. Magn. Reson., Ser A 120 (1996) 129–132.
[24] G.A. Morris, R. Freeman, Enhancement of nuclear magnetic resonance signals by polarization transfer, J. Am. Chem. Soc. 101 (1979) 760–762.
[25] M. Roth, A. Koch, P. Kindervater, J. Bargon, H.W. Spiess, K. Münnemann, C-13 hyperpolarization of a barbituric acid derivative via parahydrogen induced polarization, J. Magn. Reson. 204 (2010) 50–55.
[26] M. Goldman, H. Jóhannesson, O. Axelsson, M. Karlsson, Design and implementation of 13C hyper polarization from para-hydrogen, for new MRI contrast agents, C. R. Chim. 9 (2006) 357–363.
[27] E.Y. Chekmenev, J. Hövener, V.A. Norton, K. Harris, L.S. Batchelder, P. Bhattacharya, B.D. Ross, D.P. Weitekamp, PASADENA hyperpolarization of succinic acid for MRI and NMR spectroscopy, J. Am. Chem. Soc. 130 (2008) 4212.
[28] S. Korchak, S. Yang, S. Mamone, S. Glöggler, Pulsed magnetic resonance to signal-enhance metabolites within seconds by utilizing para-hydrogen, ChemistryOpen 7 (2018) 344–348.
[29] J. Eills, G. Stevanato, C. Bengs, S. Glöggler, S.J. Elliott, J. Alonso-Valdesueiro, G. Pileio, M.H. Levitt, Singlet order conversion and parahydrogen-induced hyperpolarization of ^{13}C nuclei in near-equivalent spin systems, J. Magn. Reson. 274 (2017) 163–172.
[30] A.N. Pravdivtsev, A.V. Yurkovskaya, N.N. Lukzen, K.L. Ivanov, H.M. Vieth, Highly efficient polarization of spin-1/2 insensitive NMR nuclei by adiabatic passage through level anticrossings, J. Phys. Chem. Lett. 5 (2014) 3421–3426.
[31] A.N. Pravdivtsev, A.V. Yurkovskaya, H. Zimmermann, H.M. Vieth, K.L. Ivanov, Transfer of SABRE-derived hyperpolarization to spin-1/2 heteronuclei, RSC Adv. 5 (2015) 63615–63623.
[32] A.S. Kiryutin, G. Sauer, S. Hadjiali, A.V. Yurkovskaya, H. Breitzke, G. Buntkowsky, A highly versatile automatized setup for quantitative measurements of PHIP enhancements, J. Magn. Reson. 285 (2017) 26–36.
[33] B.A. Rodin, K.F. Sheberstov, A.S. Kiryutin, J.T. Hill-Cousins, L.J. Brown, R.C.D. Brown, B. Jamain, H. Zimmermann, R.Z. Sagdeev, A.V. Yurkovskaya, K.L. Ivanov, Constant-adiabaticity RF-pulses for generating long-lived singlet spin states in NMR, J. Chem. Phys. 150 (2019) 064201.
[34] B.A. Rodin, A.S. Kiryutin, A.V. Yurkovskaya, K.L. Ivanov, S. Yamamoto, K. Sato, T. Takui, Using optimal control methods with constraints to generate singlet states in NMR, J. Magn. Reson. 291 (2018) 14–22.
[35] A.S. Kiryutin, G. Sauer, A.V. Yurkovskaya, H.-H. Limbach, K.L. Ivanov, G. Buntkowsky, Parahydrogen allows ultrasensitive indirect NMR detection of catalytic hydrogen complexes, J. Phys. Chem. C 121 (2017) 9879–9888.
[36] S. Knecht, A.S. Kiryutin, A.V. Yurkovskaya, K.L. Ivanov, Efficient conversion of anti-phase spin order of protons into 15N magnetisation using SLIC-SABRE, Mol. Phys. 2018 (2018) 1–10.
[37] S. Knecht, A.S. Kiryutin, A.V. Yurkovskaya, K.L. Ivanov, Mechanism of spontaneous polarization transfer in high-field SABRE experiments, J. Magn. Reson. 287 (2018) 74–81.